Some Computational Challenges in Energy Research

Victor S. Batista

Yale University, New Haven, CT, USA

1 INTRODUCTION

The development of cheap, robust, and efficient photocatalytic cells for water oxidation would allow the sustainable production of fuel from renewable resources.[1–4] An example of such a cell is shown in Figure 1, where hydrogen evolution at the cathode

$$4H^+ + 4e^- \longrightarrow 2H_2(g) \quad (1)$$

is thermodynamically driven by photoanodic water oxidation:

$$2H_2O(l) + \hbar\omega \longrightarrow O_2(g) + 4H^+ + 4e^- \quad (2)$$

The underlying photocatalytic process generates fuel (e.g., hydrogen) from water by using solar light to extract cheap electrons and protons from a renewable resource (e.g., water). The generated fuel is environmentally benign since, upon combustion, it generates only heat and water as follows:

$$4H_2(g) + O_2(g) \longrightarrow 2H_2O(l) + \Delta \quad (3)$$

The development of such type of photocatalytic solar cells based on inexpensive (e.g., earth-abundant) materials has been a long-standing challenge in photoelectrochemistry research,[5] and significant effort has been invested since the discovery of ultraviolet (UV) water oxidation on n-TiO_2 electrodes.[6] However, for many years, progress in the field has been hindered by the lack of efficient catalytic materials as well as by the lack of fundamental understanding of the processes that limit the efficiency of the conversion mechanisms.

The main challenge has been to identify catalysts able to carry out the necessary multielectron transformations at energies and rates consistent with solar irradiance. This implies designing surface-bound complexes for catalyst turnover where solar irradiance is rate limiting, activating these catalysts by multiple single-electron injection events, designing cells with redox potentials sufficiently high as to drive the desired half-reactions, and designing and assembling robust molecular components. Such a design problem requires fundamental understanding of the factors affecting the elementary steps (numbered in Figure 1), including (1) photoexcitation; (2) interfacial electron transfer (IET) and surface charge separation; (3) charge transport; (4) storage of oxidizing equivalents for catalysis; and (5) irreversible carrier collection by sacrificial acceptors, or fuel-forming reactions at the cathode. The characterization of all these processes clearly surpasses the limits of traditional disciplines and therefore calls upon researchers to establish collaborative research programs combining synthesis, computational modeling, electrochemistry, and spectroscopy.

In recent years, we have witnessed a flurry of interest in the development of catalysts for water oxidation[7–22] as well as on the development of fundamental studies of photocatalysis based on semiconductor surfaces.[23,24] Current efforts are focused on the development of more efficient catalysts based on earth-abundant materials and on molecular

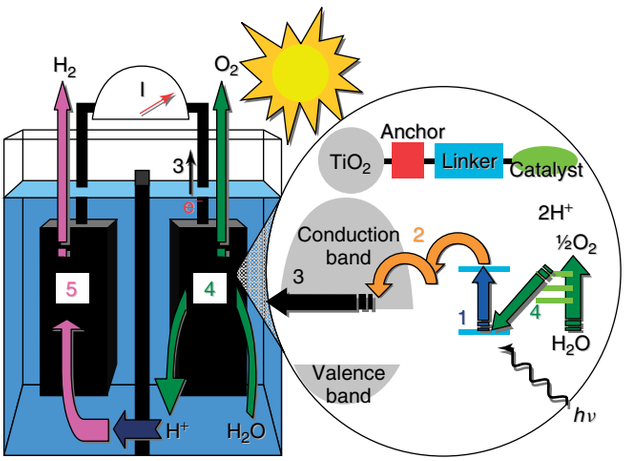

Figure 1 Photocatalytic cell for water oxidation and hydrogen evolution with schematic of elementary photoanodic processes

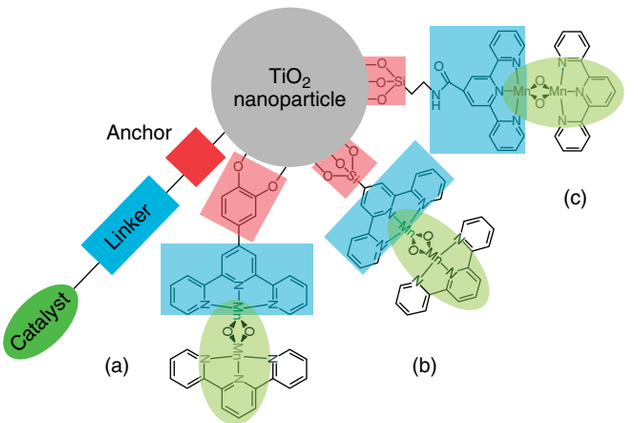

Figure 2 TiO_2 NP functionalized with Mn dimers by using various linkers including catechol (a) and siloxane-based (b and c) linkers

assemblies to efficiently couple multielectron photoanodic processes to fuel production cathodic processes. This article reviews recent advances in the field, with emphasis on computational work for the development and characterization of catalytic surfaces based on nanoporous TiO_2 thin films sensitized with manganese catalysts. The reviewed studies have been integrated with synthesis, electrochemistry, and spectroscopy in an interdisciplinary effort to advance our understanding of structure/function relationships in catalytic materials. The main aim has been to provide understanding of the fundamental processes that limit the efficiency of the reaction mechanisms and to develop guidelines for the design of novel photocatalytic materials for fuel production.

2 FUNCTIONALIZATION OF SEMICONDUCTOR SURFACES

Surface functionalization of nanoporous TiO_2 thin films is used in dye-sensitized solar cells (DSSCs) to maximize light harvesting.[25] Dye molecules on TiO_2 shift the absorption spectrum of the semiconductor to the visible region, leading to the efficient injection of electrons into the TiO_2 conduction band upon visible light absorption. The holes h^+ left behind usually have limited redox potentials since they are localized in the oxidized adsorbate molecule, rather than in the semiconductor valence band. Therefore, while efficient for light harvesting, such an approach has not led to photocatalysis.

Achieving photocatalysis with maximal light harvesting, requires sophisticated *surface catalysts* for IET. Recent studies have focused on the functionalization of TiO_2 surfaces by covalent attachment of biomimetic high-valent oxo-Mn complexes (Figure 2). These are known to be efficient catalysts for selective C–H oxygenation,[26] and water splitting to O_2.[10] Manganese catalysts are inspired by Nature, where only oxo-Mn complexes achieve redox potentials high enough to form O_2 at the oxygen-evolving complex (OEC) of photosystem II, as follows:[27–30]

$$2H_2O \longrightarrow O_2 + 4H^+ + 4e^- \quad (4)$$

The following mechanism illustrates the underlying catalytic process of water oxidation by formation of high-valent $Mn^{IV}Mn^{IV}$-O$^\bullet$ species, as illustrated for the complex $[H_2O(terpy)Mn^{III}(O)_2Mn^{IV}(terpy)H_2O]^{3+}$ (terpy, 2,2′ : 6,2″-terpyridine):

$$\textbf{Step0}: H_2O\text{-}Mn^{III}(terpy)_2Mn^{II}\text{-}OH_2 \longrightarrow H_2O\text{-}Mn^{III}(terpy)_2Mn^{III}\text{-}OH_2 + e^- \quad (5)$$

$$\textbf{Step1}: H_2O\text{-}Mn^{III}(terpy)_2Mn^{III}\text{-}OH_2 \longrightarrow H_2O\text{-}Mn^{IV}(terpy)_2Mn^{III}\text{-}OH_2 + e^- \quad (6)$$

$$\textbf{Step2}: H_2O\text{-}Mn^{IV}(terpy)_2Mn^{III}\text{-}OH_2 \longrightarrow HO\text{-}Mn^{IV}(terpy)_2Mn^{IV}\text{-}OH_2 + H^+ + e^- \quad (7)$$

$$\textbf{Step3}: HO\text{-}Mn^{IV}(terpy)_2Mn^{IV}\text{-}OH_2 \longrightarrow O{=}Mn^{V}(terpy)_2Mn^{IV}\text{-}OH_2 + H^+ + e^- \quad (8)$$

$$\textbf{Step4}: {}^\bullet O\text{-}Mn^{IV}(terpy)_2Mn^{IV}\text{-}OH_2 + 2H_2O \longrightarrow H_2O\text{-}Mn^{III}(terpy)_2Mn^{II}\text{-}OH_2 + O_2 + 2H^+ \quad (9)$$

The $Mn^{IV}Mn^{IV}$-O$^\bullet$ species is thought to be the activated form of the catalyst, normally formed by reaction of the Mn dimer with a primary oxidant (e.g., oxone), storing the four oxidizing equivalents that are necessary to oxidize water. In the photocatalytic case (Figure 1), however, such a species is formed through multiple one-electron injection processes and electron collection by the TiO_2 anode. The activation process thus avoids the use of a primary oxidant, yielding

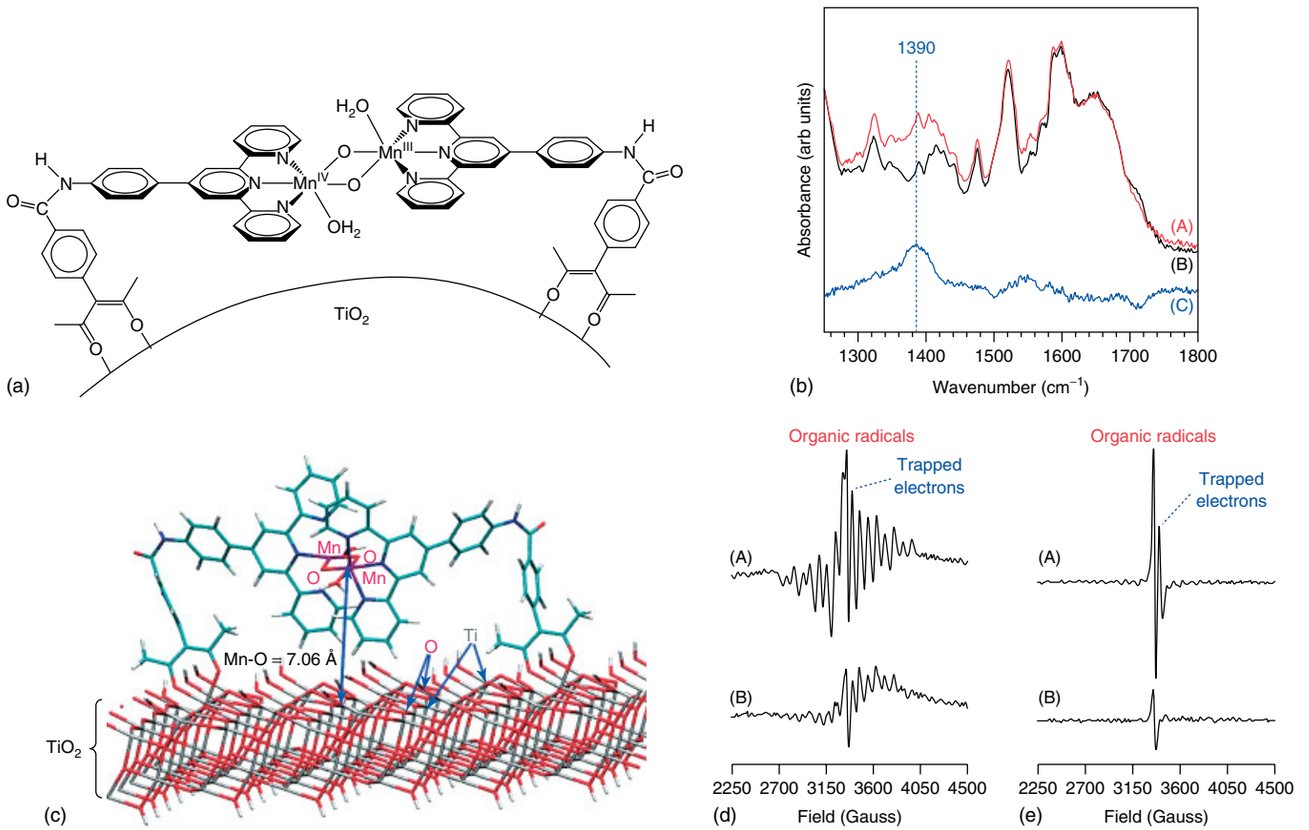

Figure 3 (a) DFT QM/MM configuration of **Mn**-L-TiO_2. (b) attenuated total reflection infrared (ATR-IR) spectra of (A) **Mn**-**L**-P25; (B) Mn^{II}-**L**-P25; and (C) shows the difference between spectra (A) and (B). (c) Resonances of organic radicals and TiO_2 lattice-trapped electrons (Ti^{3+}) are labeled. (d,e) EPR difference spectra of (A) **Mn**-**L**-P25 and (B) **Mn**-**L**-D70. (d) Light-*minus*-dark EPR spectra. (e) Postillumination dark *minus* preillumination dark EPR spectra. (Reproduced from Ref. 31. © American Chemical Society.)

a general approach for green oxidation chemistry driven by solar light.

Recent work has been focused on the direct deposition[9] as well as on the covalent attachment[31] of the Mn dimer $[H_2O(terpy)Mn^{III}(\mu\text{-}O)_2Mn^{IV}(terpy)H_2O](NO_3)_3$, (terpy, 2,2′ : 6′, 2″-terpyridine) onto nanoporous semiconductor surfaces by using a robust chromophoric linker **L**, a phenylterpy ligand attached to a 3-phenyl-acetylacetonate anchoring moiety via an amide bond (Figure 3). The resulting covalent binding to the semiconductor surface has been characterized by using quantum mechanics/molecular mechanics (QM/MM) hybrid methods in conjunction with UV–visible, IR (infrared), and EPR (electron paramagnetic resonance) spectroscopy. In addition, these studies have shown that **L** absorbs visible light, leading to photoinduced interfacial electron transfer into the semiconductor conduction band, reversibly advancing the Mn complex to the Mn(IV,IV) state. The reported work also showed that, in the absence of electron scavengers, the injected electron recombines back to form the Mn(III,IV) state in the dark.

2.1 Simulations of Interfacial Electron Transfer

Ab initio DFT (density functional theory) molecular dynamics simulations have been combined with quantum dynamics calculations of electronic relaxation to investigate IET in sensitized semiconductor nanostructures, providing fundamental understanding of IET at the detailed molecular level.[9,31–39] The characteristic times for the excited-state IET from adsorbate complexes have been shown to be consistent with terahertz experiments and with ultrafast measurements in TiO_2 sensitized by small organic molecules, including biisonicotinic acid on rutile and alizarin on TiO_2.[40,41]

2.2 Interfacial Electron Transfer

Quantum dynamics simulations have provided valuable insights on the nature of interfacial electron transfer processes leading to the activation of Mn catalysts anchored onto TiO_2 surfaces. For example, Figure 4 shows a series of snapshots for the distribution of electron density as it evolves

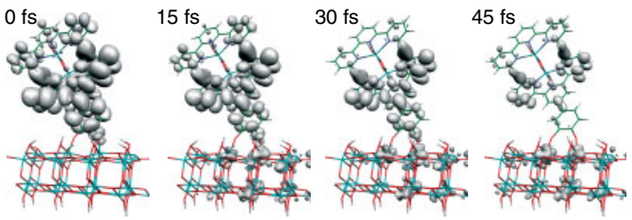

Figure 4 Snapshots, at 15-fs intervals, of the electronic charge distribution corresponding to IET after visible excitation (508 nm) of the catalyst surface complex depicted in Figure 2(a). Only the center semiconductor block is shown to allow a detailed view of the time-dependent charge distribution

during the early time dynamics of interfacial electron injection following photoexcitation of Mn dimer adsorbate. These simulations indicate that the interfacial electron injection is typically complete within an ultrafast, subpicosecond timescale when the initially populated electronic state localized in the adsorbate chromophore has suitable energy match with electronic states in the conduction band of the semiconductor surface.

Quantum dynamics simulations of interfacial electron transfer solve the time-dependent Schrödinger equation, yielding a detailed description of the time-dependent charge distribution after photoexcitation of the adsorbate. The resulting charge distribution provides information on the electronic orbitals responsible for hosting the injected electron in the semiconductor host substrate as well as the evolution of the spatial distribution of electronic population as it relaxes in the semiconductor conduction band. This type of atomistic simulations have also provided a description of the influence of thermal fluctuations on the underlying relaxation pathways.[33] Simulation studies beyond the low-temperature analysis have analyzed room-temperature conditions typical of photocatalytic cells, showing that thermal nuclear fluctuations can speed up the underlying interfacial electron transfer dynamics. The molecular/electronic origin of such effects has been traced to fluctuations that break the symmetry of otherwise orthogonal electronic states, creating additional relaxation pathways for carrier diffusion. Analogous computer simulations have also allowed the detailed analysis of the relaxation dynamics of holes, localized the monolayer of adsorbate molecules, created upon photoexcitation and interfacial electron transfer of sensitized TiO_2 nanoparticles (NPs) under cryogenic temperature conditions.[34,42]

3 PROTON-COUPLED ELECTRON TRANSFER

Proton-coupled electron transfer (PCET) is often essential to achieve high catalytic turnovers of multielectron redox processes. Protonation/deprotonation processes can

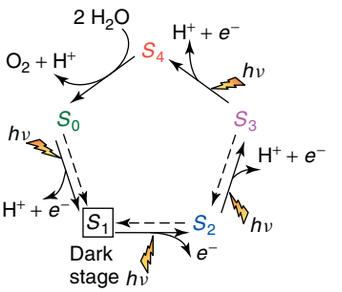

Figure 5 Catalytic cycle proposed by Joliot and Kok for water splitting into dioxygen, protons, and electrons at the OEC in PSII [1,2]. Dashed arrows indicate spontaneous interconversion processes in the dark. The steps for substrate water attachment and proton release are only tentatively proposed and might change with pH

facilitate reduction/oxidation state transitions, preventing charge buildup during the accumulation of multiple reducing (or oxidizing) equivalents. For example, PCET is thought to play an important role in keeping all of the redox steps in the Kok's catalytic cycle of water oxidation (Figure 5),[43,44] over a narrow range of potential at ~1 V. The resulting ''redox-leveling'' effect prevents the accumulation of charge in the catalytic complex, allowing for the accumulation of four oxidizing equivalents in the OEC, embedded in the low dielectric environment of photosystem II (PSII).

The design of efficient catalysts for water oxidation often aims to develop molecular frameworks where the reactivity mimics the catalytic functionality of the OEC, leading to reaction pathways where the redox-leveling effect is induced by PCET. However, general design principles for efficient PCET mechanisms are still lacking. Computational modeling can play an important role in understanding catalytic processes of natural systems (e.g., photosystem II),[11,12,45–51] as well as on the design and characterization of catalysts with similar functionality, by guiding the selection of suitable ligands for transition metal complexes that lead to redox-leveling mechanisms based on PCET. Recent studies of biomimetic oxomanganese complexes have been based on rigorous quantum chemistry calculations of redox potentials and pK_a values and direct comparisons with electrochemical measurements.[52]

Figure 6 shows results of calculations of free energy changes associated with the oxidation state transition (III,III) → (III,IV) in the mixed-valent Mn complex $[(bpy)_2Mn^{III}(\mu\text{-}O)_2Mn^{IV}(bpy)_2]^{3+}$ (bpy, 2,2′-bipyridyl), as obtained at the DFT B3LYP/cc-pVTZ(-f) level by using the standard thermodynamic cycle formalism applied in conjunction with continuum solvation models.[52] It is shown that the pK_a values of the oxo-ligands depend strongly on the oxidation states of the complex, changing by approximately 10 pH units (i.e., from pH ~ 2 to pH ~ 12) upon III,IV → III,III reduction of the Mn complex. These results are in good agreement with the experimental pK_a values determined by solution

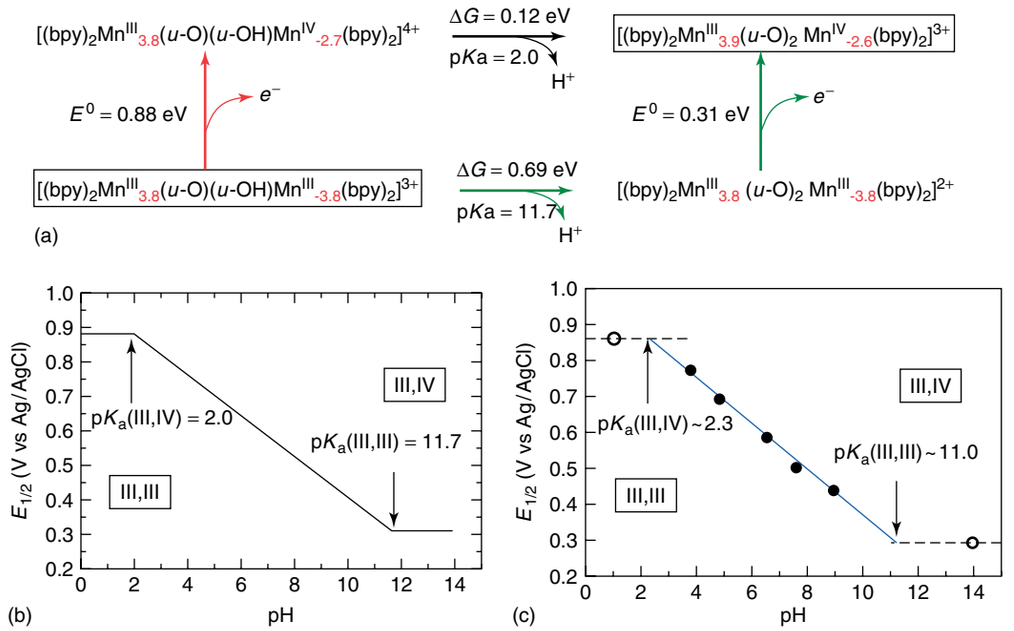

Figure 6 (a) Thermodynamic energy diagram of PCET for complex **1** in aqueous solutions at pH = 0, as described by DFT B3LYP/cc-pVTZ(-f) free energy calculations of redox potentials and pK_a values based on the Haber-Born cycle method applied in conjunction with a continuum solvation model. Formal oxidation numbers are indicated as superscripts in Roman numbers and the spin populations obtained according to the Mulliken population analysis are indicated as subscripts in red. (b) Pourbaix diagram for complex 1 in aqueous solutions, obtained (b) from free energy calculations of redox potentials at the DFT B3LYP/cc-pVTZ(-f) level of theory, and (c) experimental data (the circles). (Reproduced from Ref. 54. © American Chemical Society.)

magnetic susceptibility and near-IR spectroscopy,[53] as well as with the pH dependence of the redox potential previously reported by cyclic voltammogram (CV) measurements,[54] and provide fundamental understanding of the underlying changes in protonation and oxidation states leading to the pH dependence of redox potentials.

Figure 6(a) shows that the protonated reduced species $\mathbf{1_{red}}$ $[(bpy)_2Mn^{III}(\mu\text{-}O)(\mu\text{-}OH)Mn^{III}(bpy)_2]^{3+}$ can be oxidized via two possible pathways, including oxidation by a direct ionization process requiring a rather high free energy change of 0.88 eV (red arrow), or oxidation by the concerted removal of an electron from the complex and a proton from the μ-hydroxo bridge (green arrow). These results indicate that the underlying oxidation is strongly coupled to deprotonation of the μ-OH bridge for a wide range of values of pH (i.e., pH = 2.0–11.7). For $\mathbf{1_{red}}$, the oxidation free energy is constant (~0.88 V) at pH < 2.0 (oxidation takes the red path). Within the 2.0 < pH < 11.7 range, the overall free energy requirement consists of two parts, including 0.69−0.059*pH eV for the deprotonation step and an extra 0.31 eV for the oxidation of the deprotonated species. Finally, at pH > 11.7, the oxidation free energy becomes constant since the green path dominates with spontaneous deprotonation.

Figure 6(b,c) shows the comparison of Pourbaix diagrams, illustrating the pH dependence of $E_{1/2}$, as computed at the DFT B3LYP/cc-pVTZ(-f) level of theory and directly compared to CV measurements.[54] The agreement shows that theory can provide accurate descriptions of the regulatory effect of reduction state transitions on the pK_a values of the ligands and the effect of protonation of oxo-ligands on the redox potentials of metal centers. Therefore, it is natural to expect that analogous calculations and direct comparisons to experimental data will allow the study of PCET along the catalytic cycle of multielectron reactions catalyzed by other transition metal complexes.

4 RECTIFICATION OF INTERFACIAL ELECTRON TRANSFER

A common problem to any scheme where photoexcitation creates an electron-hole pair state is electron-hole pair recombination. In PSII, recombination is suppressed by an arrangement of redox cofactors that induce directionality of electron transfer after the initial charge separation. Molecular diodes can also induce directionality of electron transfer[55] and have been recently explored in the design of semiconductor materials where the covalent attachment of molecular linkers induces rectification of interfacial electron transfer (Figure 7). The electronic rectification properties of molecular linkers that covalently bind Mn catalysts to TiO_2 surfaces, including

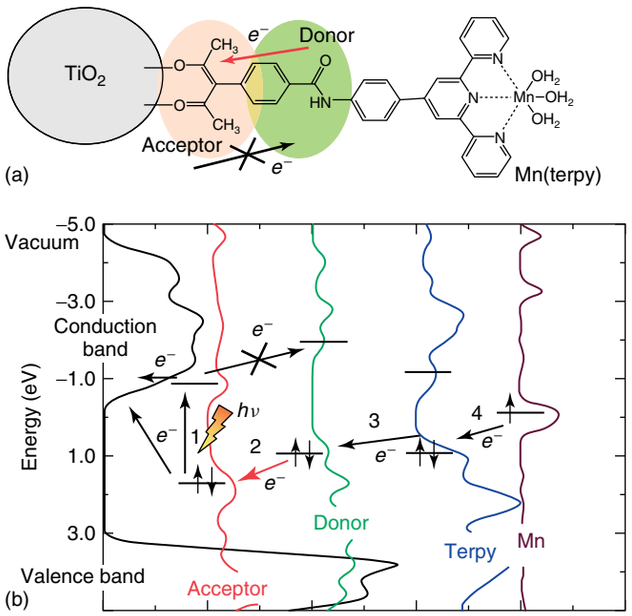

Figure 7 (a) Schematic diagram of a TiO_2 NP functionalized with $[Mn^{II}(H_2O)_3]^{2+}$, where the Mn complex is covalently attached to the TiO_2 surface by the phenyl-acac anchor. (b) Density of electronic states and arrows indicating the electron transfer pathway, induced by photoexcitation and electron injection, leading to Mn oxidation. Favorable directionality of electron transfer is due to the positioning of electronic energy levels in the electron donor and acceptor parts of the ligand-linker chromophore. (Reproduced from Ref. 36. © American Chemical Society.)

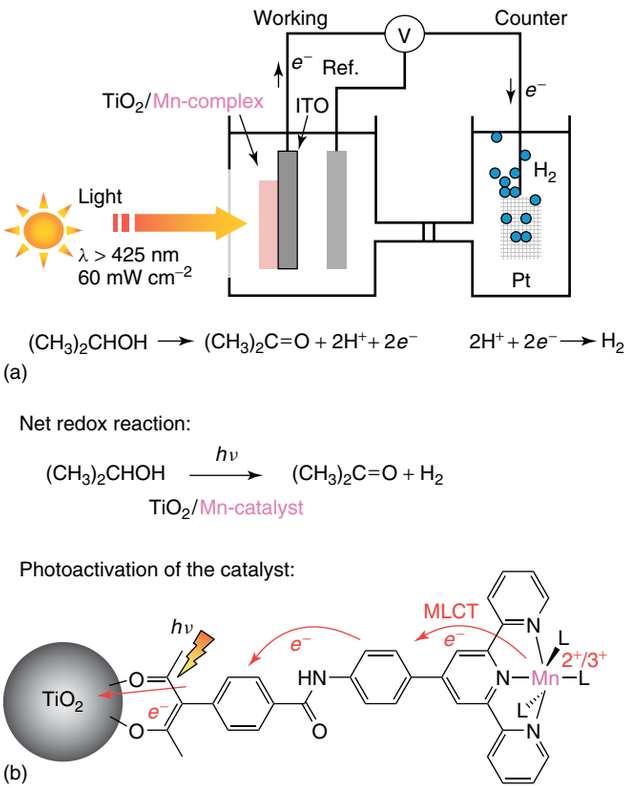

Figure 8 Photocatalytic cell for visible-light-driven oxidation chemistry and H_2 evolution (a), based on TiO_2 thin-film photoanodes functionalized with Mn catalysts covalently attached via chromophoric linkers (b)

Mn-complexes with phenylterpyridine ligands attached to 3-phenyl-acetylacetonate anchors via amide bonds, have been characterized by calculations of current–voltage characteristics at metallic junctions.[56] It was found that a suitable choice of the amide linkage can induce directionality of interfacial electron transfer. These findings were consistent with EPR measurements, confirming an asymmetry of electron transfer rates for linkers with significant rectification.[56] These studies are particularly relevant for the development of photovoltaic or photocatalytic devices based on functionalized TiO_2 thin films where the overall performance is often affected by recombination processes competing with interfacial electron injection.

Calculations of current–voltage *(I–V)* characteristics were performed with the software package SMEAGOL,[57,58] integrating the nonequilibrium Green's function (NEGF) method[59,60] with DFT[61] as implemented in the SIESTA package for electronic structure calculations.[62] The systems were modeled in the usual three-subsystem segmentation with the molecular diode of interest in between metallic electrodes.[56] The surface Green's functions, describing the current–voltage probes, were obtained as a direct summation of both open and closed scattering channels together with a regularization procedure of the Hamiltonian that provides a significant improvement over standard recursive methods.

5 FUEL FORMATION

Recent work on photocatalytic cells based on TiO_2 thin-film photoanodes functionalized with Mn-complexes has focused on coupling H_2 evolution driven to photoanodic oxidation reactions. Figure 8 shows a schematic diagram of a specific photocatalytic cell based on TiO_2 electrodes functionalized with Mn-terpy catalysts that can couple hydrogen evolution with oxidation of isopropanol to acetone. The reaction is catalyzed by the Mn-terpy complex adsorbate, activated by interfacial electron injection into the TiO_2 host substrate, upon absorption of visible light ($\lambda > 425$ nm).[63] The activation process induces the oxidation-state transition Mn(II) → Mn(III) in the metal center, generating Mn(III) with sufficient oxidizing power to transform isopropanol in acetone. The injected electrons are combined with protons in the counter-electrode to produce hydrogen. It has been shown that such a mechanism, involving photoexcitation, interfacial electron injection, charge carrier collection, and irreversible hydrogen evolution, can be accomplished when the Mn-terpy catalysts are covalently attached to the TiO_2 surface by using robust chromophoric linkers that are stable in aqueous solutions under oxidative conditions.

Similar results have been reported for other ''proof-of-concept'' visible-light-driven photocatalytic cells, including cells based on other (although more expensive) transition metal catalysts,[13,24] indicating that the functionalization of semiconductor surfaces by covalent attachment of transition metal complexes yields a general approach for the development of photocatalytic solar cells.

6 CONCLUSIONS

The emergence of photocatalytic solar cells based on semiconductor materials functionalized with earth-abundant transition metal complexes represent a promising development for the sustainable production of fuel from renewable resources (e.g., water). Recent advances in the study of fundamental aspects that affect the overall efficiency of the underlying catalytic mechanisms suggest that control over photoabsorption, PCET, and IET can be achieved by implementing the ligand design methodology that has been so successful for many years in the development of homogeneous catalysts. When fundamentally informed by structural and mechanistic characterization based on computational modeling, high-resolution spectroscopy, and electrochemistry, in conjunction with the comparative analysis of analogous catalytic processes in nature, the resulting methodology constitutes a powerful ''bottom-up'' synthetic tool for the development of new catalytic materials. These emerging methods are thus expected to continue making significant contributions in the development of novel semiconductor materials for photocatalytic solar cells.

7 RELATED ARTICLES

Dye-Sensitized Solar Cells: an Overview; Energy Conversion in Photosynthesis; Hydrogen Economy; Molecular Catalysis for Fuel Cells; Molecular Catalysts for Oxygen Production from Water; Photocatalytic Hydrogen Production from Water; Toward Solar Fuels Using a Biomimetic Approach: Progress in the Swedish Consortium for Artificial Photosynthesis; Recent Advances in Photo-Initiated Electron-Transfer at the Interface between Anatase TiO_2 Nanocrystallites and Transition-Metal Polypyridyl Compounds.

8 ABBREVIATIONS AND ACRONYMS

CV = cyclic voltammogram; DFT = density functional theory; DSSC = dye-sensitized solar cells; EPR = electron paramagnetic resonance; IET = interfacial electron transfer; IR = infrared; NEGF = nonequilibrium green's function; NP = nanoparticle; OEC = oxygen-evolving complex; PCET = proton coupled to electron transfer; QM/MM = quantum mechanics/molecular mechanics; UV = ultraviolet.

9 REFERENCES

1. A. J. Bard and M. A. Fox, *Acc. Chem. Res.*, 1995, **28**, 141.
2. E. E. Benson, C. P. Kubiak, A. J. Sathrum, and J. M. Smieja, *Chem. Soc. Rev.*, 2009, **38**, 89.
3. A. J. Morris, G. J. Meyer, and E. Fujita, *Acc. Chem. Res.*, 2009, **42**, 1983.
4. M. Rakowski-Dubois and D. L. Dubois, *Acc. Chem. Res.*, 2009, **42**(12), 1974.
5. A. J. Bard and M. A. Fox, *Acc. Chem. Res.*, 1995, **28**, 141.
6. A. Fujishima and K. Honda, *Nature*, 1972, **238**, 37.
7. N. D. McDaniel, F. J. Coughlin, L. L. Tinker, and S. Bernhard, *J. Am. Chem. Soc.*, 2008, **130**, 210.
8. J. F. Hull, D. Balcells, J. D. Blakemore, C. D. Incarvito, O. Eisenstein, G. W. Brudvig, and R. H. Crabtree, *J. Am. Chem. Soc.*, 2009, **131**, 8730.
9. G. H. Li, E. M. Sproviero, R. C. Snoeberger, N. Iguchi, J. D. Blakemore, R. H. Crabtree, G. W. Brudvig, and V. S. Batista, *Energy Environ. Sci.*, 2009, **2**, 230.
10. J. Limburg, J. S. Vrettos, L. M. Liable-Sands, A. L. Rheingold, R. H. Crabtree, and G. W. Brudvig, *Science*, 1999, **283**, 1524.
11. E. M. Sproviero, J. A. Gascon, J. P. McEvoy, G. W. Brudvig, and V. S. Batista, *Curr. Opin. Struct. Biol.*, 2007, **17**, 173.
12. E. M. Sproviero, J. A. Gascon, J. P. McEvoy, G. W. Brudvig, and V. S. Batista, *Coord. Chem. Rev.*, 2008, **252**, 395.
13. W. J. Youngblood, S. H. A. Lee, K. Maeda, and T. E. Mallouk, *Acc. Chem. Res.*, 2009, **42**, 1966.
14. M. W. Kanan and D. G. Nocera, *Science*, 2008, **321**, 1072.
15. M. W. Kanan, Y. Surendranath, and D. G. Nocera, *Chem. Soc. Rev.*, 2009, **38**, 109.
16. Z. F. Chen, J. J. Concepcion, J. W. Jurss, and T. J. Meyer, *J. Am. Chem. Soc.*, 2009, **131**, 15580.
17. J. J. Concepcion, J. W. Jurss, M. K. Brennaman, P. G. Hoertz, A. O. T. Patrocinio, N. Y. M. Iha, J. L. Templeton, and T. J. Meyer, *Acc. Chem. Res.*, 2009, **42**, 1954.
18. J. J. Concepcion, J. W. Jurss, M. R. Norris, Z. F. Chen, J. L. Templeton, and T. J. Meyer, *Inorg. Chem.*, 2010, **49**, 1277.
19. S. W. Gersten, G. J. Samuels, and T. J. Meyer, *J. Am. Chem. Soc.*, 1982, **104**, 4029.
20. R. Brimblecombe, A. M. Bond, G. C. Dismukes, G. F. Swiegers, and L. Spiccia, *PCCP*, 2009, **11**, 6441.
21. R. Brimblecombe, G. F. Swiegers, G. C. Dismukes, and L. Spiccia, *Angew. Chem.-Int. Ed.*, 2008, **47**, 7335.

22. G. C. Dismukes, R. Brimblecombe, G. A. N. Felton, R. S. Pryadun, J. E. Sheats, L. Spiccia, and G. F. Swiegers, *Acc. Chem. Res.*, 2009, **42**, 1935.
23. A. Mills and S. Le Hunte, *J. Photochem. Photobiol.*, 1997, **108**, 1.
24. J. A. Treadway, J. A. Moss, and T. J. Meyer, *Inorg. Chem.*, 1999, **38**, 4386.
25. B. ORegan and M. Gratzel, *Nature*, 1991, **353**, 737.
26. S. Das, C. D. Incarvito, R. H. Crabtree, and G. W. Brudvig, *Science*, 2006, **312**, 1941.
27. R. Manchanda, G. W. Brudvig, and R. H. Crabtree, *Coord. Chem. Rev.*, 1995, **144**, 1.
28. E. M. Sproviero, J. A. Gascon, J. P. McEvoy, G. W. Brudvig, and V. S. Batista, *J. Chem. Theory Comput.*, 2006, **2**, 1119.
29. J. Limburg, J. S. Vrettos, H. Y. Chen, J. C. de Paula, R. H. Crabtree, and G. W. Brudvig, *J. Am. Chem. Soc.*, 2001, **123**, 423.
30. E. M. Sproviero, J. A. Gascon, J. P. McEvoy, G. W. Brudvig, and V. S. Batista, *J. Inorg. Biochem.*, 2006, **100**, 786.
31. G. Li, E. M. Sproviero, W. R. McNamara, R. C. Snoeberger, R. H. Crabtree, G. W. Brudvig, and V. S. Batista, *J. Phys. Chem. B*, 2010, DOI: 10.1021/jp908925z (Submitted).
32. L. G. C. Rego and V. S. Batista, *J. Am. Chem. Soc.*, 2003, **125**, 7989.
33. S. G. Abuabara, L. G. C. Rego, and V. S. Batista, *J. Am. Chem. Soc.*, 2005, **127**, 18234.
34. L. G. C. Rego, S. G. Abuabara, and V. S. Batista, *J. Chem. Phys.*, 2005, **122**(15), 122.
35. S. Jin, R. C. Snoeberger, A. Issac, V. S. Batista, and T. Lian, *J. Phys. Chem. B*, 2010, DOI: 10.1021/jp911662g (Submitted).
36. W. R. McNamara, R. C. Snoeberger, G. Li, J. M. Schleicher, C. W. Cady, M. Poyatos, C. A. Schmuttenmaer, R. H. Crabtree, G. W. Brudvig, and V. S. Batista, *J. Am. Chem. Soc.*, 2008, **130**, 14329.
37. W. R. McNamara, R. C. Snoeberger, G. H. Li, C. Richter, L. J. Allen, R. L. Milot, C. A. Schmuttenmaer, R. H. Crabtree, G. W. Brudvig, and V. S. Batista, *Energy Environ. Sci.*, 2009, **2**, 1173.
38. L. G. C. Rego, R. da Silva, J. A. Freire, R. C. Snoeberger, and V. S. Batista, *J. Phys. Chem. C*, 2010, **114**, 1317.
39. R. C. Snoeberger, T. Lian, and V. S. Batista, *Proc. SPIE*, 2010, **7396**, 739604.
40. R. Huber, J. E. Moser, M. Gratzel, and J. Wachtveitl, *J. Phys. Chem. B*, 2002, **106**, 6494.
41. J. Schnadt, P. A. Bruhwiler, L. Patthey, J. N. O'Shea, S. Sodergren, M. Odelius, R. Ahuja, O. Karis, M. Bassler, P. Persson, H. Siegbahn, S. Lunell, and N. Martensson, *Nature*, 2002, **418**, 620.
42. L. G. C. Rego, S. G. Abuabara, and V. S. Batista, *Quantum Inf. Comput.*, 2005, **5**, 318.
43. P. Joliot, G. Barbieri, and R. Chabaud, *Photochem. Photobiol.*, 1969, **10**, 309.
44. B. Kok, B. Forbush, and M. McGloin, *Photochem. Photobiol.*, 1970, **11**, 457.
45. E. M. Sproviero, J. A. Gascon, J. P. McEvoy, G. W. Brudvig, and V. S. Batista, *J. Chem. Theory Comput.*, 2006, **2**, 1119.
46. E. M. Sproviero, J. A. Gascon, J. P. McEvoy, G. W. Brudvig, and V. S. Batista, *J. Inorg. Biochem.*, 2006, **100**, 786.
47. E. M. Sproviero, J. A. Gascon, J. P. McEvoy, G. W. Brudvig, and V. S. Batista, *J. Am. Chem. Soc.*, 2008, **130**, 6728.
48. E. M. Sproviero, J. A. Gascon, J. P. McEvoy, G. W. Brudvig, and V. S. Batista, *J. Am. Chem. Soc.*, 2008, **130**, 3428.
49. E. M. Sproviero, J. P. McEvoy, J. A. Gascon, G. W. Brudvig, and V. S. Batista, *Photosynth. Res.*, 2008, **97**, 91.
50. E. M. Sproviero, M. B. Newcomer, J. A. Gascon, E. R. Batista, G. W. Brudvig, and V. S. Batista, *Photosynth. Res.*, 2009, **102**, 455.
51. E. M. Sproviero, K. Shinopoulos, J. A. Gascon, J. P. McEvoyO, G. W. Brudvig, and V. S. Batista, *Philos. Transa. R. Soc. B-Biol. Sci.*, 2008, **363**, 1149.
52. T. Wang, G. Brudvig, and V. S. Batista, *J. Chem. Theory Comput.*, 2010, **6**, 755.
53. S. R. Cooper and M. Calvin, *J. Am. Chem. Soc.*, 1977, **99**, 6623.
54. H. H. Thorp, J. E. Sarneski, G. W. Brudvig, and R. H. Crabtree, *J. Am. Chem. Soc.*, 1989, **111**, 9249.
55. M. Elbing, R. Ochs, M. Koentopp, M. Fischer, C. von Hanisch, F. Weigend, F. Evers, H. B. Weber, and M. Mayor, *Proc. Natl. Acad. Sci. U.S.A.*, 2005, **102**, 8815.
56. J. A. Palma, W. R. McNamara, R. C. Snoeberger, C. Richter, R. L. Milot, C. A. Schmuttenmaer, R. H. Crabtree, G. W. Brudvig, and V. S. Batista, *J. Am. Chem. Soc.*, 2010, submitted.
57. A. R. Rocha, V. Garcia-Suarez, S. W. Bailey, C. J. Lambert, and J. S. S. Ferrer, *J. Chem. Phys.*, 2005, **4**, 335.
58. A. R. Rocha, V. Garcia-Suarez, S. W. Bailey, C. J. Lambert, J. Ferrer, and S. Sanvito, *Phys. Rev. B*, 2006, **73**, 085414.
59. L. V. Keldysh, *Sov. Phys. JETP*, 1965, **20**, 1018.
60. S. Datta, 'Electronic Transport in Mesoscopic Systems', Cambridge University Press, Cambridge, 1997.
61. W. Kohn and L. J. Sham, *Phys. Rev. A*, 1965, **140**(4A), 1133.
62. J. M. Soler, E. Artacho, J. D. Gale, A. Garcia, J. Junquera, P. Ordejon, and D. Sanchez-Portal, *J. Phys. Cond. Matt.*, 2002, **14**, 2745.
63. G. Li, W. R. McNamara, R. C. Snoeberger, R. H. Crabtree, G. W. Brudvig, and V. S. Batista, *J. Am. Chem. Soc.*, 2010, submitted.